



Title	Field dependence of coupling efficiency between electromagnetic field and ultrasonic bulk waves
Author(s)	Ogi, Hirotsugu
Citation	Journal of Applied Physics. 1997, 82(8), p. 3940-3949
Version Type	VoR
URL	<a href="https://hdl.handle.net/11094/84231">https://hdl.handle.net/11094/84231</a>
rights	This article may be downloaded for personal use only. Any other use requires prior permission of the author and AIP Publishing. This article appeared in Journal of Applied Physics, 82(8), 3940-3949 (1997) and may be found at <a href="https://doi.org/10.1063/1.365701">https://doi.org/10.1063/1.365701</a> .
Note	

*The University of Osaka Institutional Knowledge Archive : OUKA*

<https://ir.library.osaka-u.ac.jp/>

The University of Osaka

# Field dependence of coupling efficiency between electromagnetic field and ultrasonic bulk waves

Hirotsugu Ogi<sup>a)</sup>

*Graduate School of Engineering Science, Osaka University, Toyonaka, Osaka 560, Japan*

(Received 5 May 1997; accepted for publication 4 July 1997)

The coupling mechanism of the electromagnetic acoustic transducer (EMAT) for bulk waves has been studied by examining the magnetic-field dependence of the wave amplitudes. A spiral elongated coil placed on a thin plate of low carbon steel excites and receives the longitudinal and the shear waves propagating in the thickness direction in the presence of the bias magnetic field. The field dependences of the bulk-wave amplitudes are measured using the electromagnetic acoustic resonance both for the normal and tangential bias fields, which showed different features, depending on the bias-field direction and the wave mode. A two-dimensional model is presented for the explanation of the observed results. The present analysis emphasizes the inclined total field in the derivation of the magnetostriction constants, which is revealed to play an essential role for the wave generation. Both the measurement and the model analysis conclude that the magnetostrictive effect dominates the EMAT phenomena for the bulk waves in ferromagnetic metal, regardless of the bias field direction. © 1997 American Institute of Physics. [S0021-8979(97)02220-2]

## I. INTRODUCTION

An electromagnetic acoustic transducer (EMAT) has definite advantages for the nondestructive inspection and materials characterization of electrically conductive materials.<sup>1-12</sup> The EMATs generate and detect the ultrasonic elastic waves by means of the electromagnetic transduction and need no coupling materials, which eliminate measurement errors associated with the contacting transduction. They generally consist of permanent magnets (or electromagnets) to supply the bias magnetic field, and the driving coil element to excite the eddy currents and the dynamic fields. Their configurations depend on the modes of elastic waves to be excited.

For the optimum performance of an EMAT for the materials characterization, it is important to understand the coupling mechanism between the electromagnetic fields and the elastic waves. This has been a long running topic in the area of the ultrasonics and electromagnetic physics. This article is devoted to studying the coupling mechanism of the bulk-wave generation and reception by an EMAT through the investigation of the dependence of the detected wave amplitudes on the bias-magnetic field. Previous work<sup>5-8</sup> concluded that three mechanisms are responsible for the coupling; they are the Lorentz force mechanism due to the interaction between the induced eddy current and the bias flux density, the magnetization force mechanism due to the bias magnetization, and the magnetostriction mechanism due to the piezomagnetic effect in a ferromagnetic material. The Lorentz force arises in any conducting material, while the other two forces occur only in ferromagnetic materials. For nonmagnetic metals, the transduction is well understood as the Lorentz force mechanism, but it is highly complex in case of a ferromagnetic material. Thompson<sup>5</sup> had studied the field dependence of the guided-wave amplitude in ferromagnetic plates and derived a theoretical model to explain the results.

Il'in and Kharitonov<sup>6</sup> calculated the receiving efficiency for the Rayleigh waves by a meanderline coil in a ferromagnetic metal. Wilbrand<sup>7,8</sup> presented more detailed discussion on the bulk wave detection involving the three mechanisms. They concluded that when the static field is parallel to the sample surface, the magnetostrictive effect dominates, while for the normal field to the surface, the magnetostrictive effect contributes little and the other two mechanisms serve to the wave generation and reception. The theoretical model presented by Wilbrand<sup>8</sup> is well acceptable, but his conclusion for the case of the normal bias field seems to be insufficient from an experimental viewpoint. He verified his calculation through the measurement of the directivity pattern of the receiving efficiency of the (SV) wave. Such a measurement looks at only an aspect of the phenomena and is insufficient for the full understanding.

Study on the field dependence of the wave amplitudes provides a pertinent access to clarify the coupling mechanism. The field dependences of the Lorentz force and the magnetization force will be proportional to the magnetization, and that of the magnetostrictive force will be governed by the magnetostriction curve. They show different dependences on the bias field. Such a measurement has to be performed for a thin plate to establish the high grade of field homogeneity in the sample. But, the usual pulse-echo technique is unavailable because of the overlapping of echoes. Therefore, we use the technique of the electromagnetic acoustic resonance (EMAR)<sup>9-13</sup> to measure the bulk-wave amplitude from a peak height of the resonant spectrum.

This article presents the model analysis on the field dependence of the bulk-wave generation and reception by a spiral elongated coil. Following the existing work, a two-dimensional model is used to estimate the coupling efficiency. It emphasizes the spatial change of the total field composed of the bias field and the dynamic field in the calculation of the magnetostriction constants. This effect plays an essential role in the bulk wave generation, but it has not

<sup>a)</sup>Electronic mail: ogi@me.es.osaka-u.ac.jp

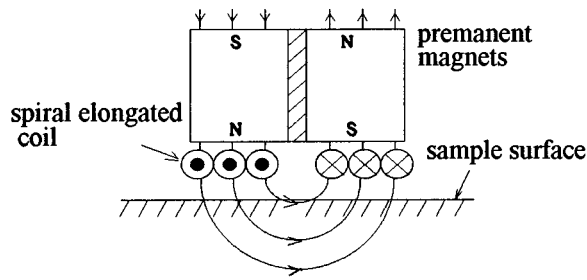


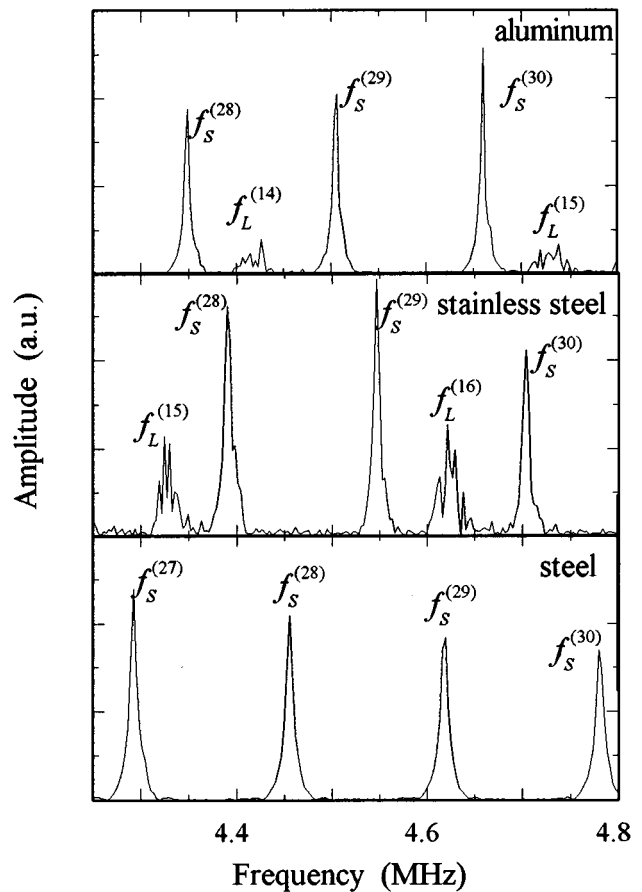
FIG. 1. Configuration of the bulk-wave EMAT.

been taken into account in the previous work. The calculation is compared with the measurement by the EMAR technique. We conclude that the magnetostrictive mechanism dominates the bulk wave generation and reception, especially, for the shear wave case, regardless of the bias-field direction. This analysis gives an answer for unsolved behaviors associated with a bulk-wave EMAT and will help us to design new types of EMATs for potential applications in ferromagnetic metals.

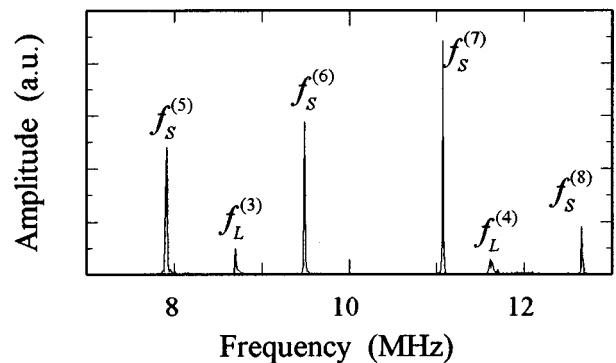
## II. TYPICAL BEHAVIOR OF A BULK-WAVE EMAT

The bulk-wave EMAT illustrated in Fig. 1 has a compact and robust structure, and is most often used in the practical applications by detecting bulk waves propagating normal to the surface.<sup>9,10,12</sup> It consists of a spiral elongated coil and a pair of permanent magnets on the coil. The magnets produce the normal field to the surface under the coil elements and the tangential field around the center and the edges of the coil elements. It is an experimental fact that this EMAT generates both the shear and the longitudinal waves in a non-magnetic metal, but it generates only the shear wave in a ferromagnetic metal; the longitudinal wave is too weak to be observed. Figure 2 shows the EMAR spectra<sup>10</sup> measured with a bulk-wave EMAT for several metal plates. The results demonstrate that in the nonmagnetic metals, both the shear and longitudinal waves are detected, but for the ferromagnetic metal it detects only the shear wave when the sample is thick; for the thinner plate, it detects the longitudinal wave as well.

In the surface region under the coil elements, the Lorentz forces occur parallel to the surface due to the interaction between the normal bias field from the magnets and the eddy currents induced by the driving current, being sources of the shear waves. For the nonmagnetic metals, the Lorentz force also explains the longitudinal-wave generation as a result of the interaction between the tangential bias field around the center of the coil and the eddy current. The existing work<sup>5,6</sup> showed that in a ferromagnetic metal magnetized by the tangential field, the major part of the vertical Lorentz force is canceled by the magnetization force. Certainly, this fact could be an explanation of much smaller coupling efficiency in the longitudinal wave generation. But, it fails to explain why the efficiency is increased for the thinner plate. Furthermore, the existing work concludes that the magnetostriction force is considerable in the presence of the tangential field. If so, the magnetostriction effect would cause the vertical body



(a) EMAR spectra from plates of 10-mm thick



(b) EMAR spectrum from a 1-mm thick steel plate.

FIG. 2. EMAR spectra detected by a bulk-wave EMAT with the plates of an aluminum, an austenitic stainless steel, and a low carbon steel; (a) 10-mm-thick plates, and (b) 1-mm-thick carbon steel plate.  $f_S^{(n)}$  and  $f_L^{(n)}$  denote the  $n$ th resonant frequencies of the shear and longitudinal waves, respectively. The normal component of the magnetic field is 0.3–0.5 T near the magnet poles, and the parallel component is 0.4 to 0.5 T.

force in the center region and could be a source to generate the longitudinal wave. However, the longitudinal wave is hardly detected in practice. These contradiction associated with the bulk-wave EMAT will be solved by the following experiments and the theoretical analysis.

## III. MEASUREMENT OF FIELD DEPENDENCE

A spiral elongated coil is placed on a sample surface and the bias magnetic field is supplied parallel or normal to the

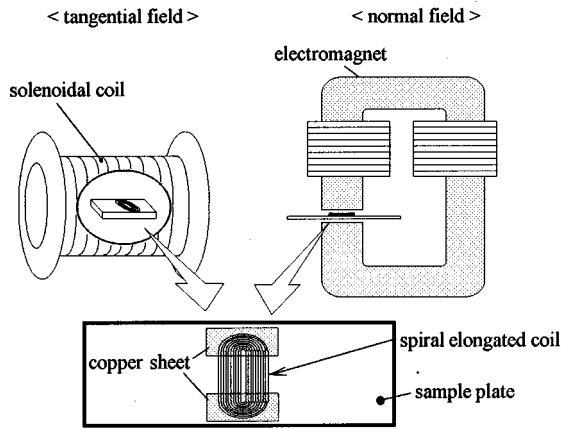


FIG. 3. Configurations for measuring the field dependence with the spiral elongated coil and bias fields.

surface. Figure 3 shows the setup of the measurements. Sample plate is a low carbon steel, being sized  $100^l \times 30^w \times 3^t$  mm<sup>3</sup>. The solenoidal coil gives the parallel field to the surface up to 0.8 kOe and the electromagnet gives the normal field up to 1.2 T. The bias fields in the sample are measured by the hole sensor attached on the surface on the basis of their continuity across the surface. The spiral elongated coil is fabricated by printing copper on a polyimide sheet. A part of the coil face of the sample side is shielded with copper sheets (0.045 mm thick) to make only the straight parts active. The active area of the coil is  $10 \times 10$  mm<sup>2</sup>.

The coil is driven by the high-power rf bursts with 40  $\mu$ s duration, gated coherently, to generate the bulk waves which are propagated and reflected in the sample. The same coil receives the reverberation made up with the overlapping multiple echoes of various phases. The received signal is processed to acquire the spectroscopic response by measuring the amplitude as a function of the operating frequency.<sup>10</sup> Only at a resonance, many reflection echoes are received in phase and their amplitudes are summed up to give an easily measurable intensity, compensating in excess for the low efficiency with the EMAT. The resonant spectrum shows a series of sharp peaks at the discrete resonant frequencies, which are  $f^{(n)} = nc/(2d)$  for a plate of thickness  $d$ ;  $c$  is the longitudinal or shear wave velocity and  $n$  the integer representing the resonant order. The wave amplitudes are determined from the peak heights of the resonant spectra. All the measurements were performed after cyclic demagnetization; that is, the magnetization always progresses along the initial magnetization curve.

Figure 4 shows an example of the measured resonant spectrum of the steel plate for the tangential bias field of 0.18 kOe. Measurement of the field dependences is made on the resonant spectra of the fourth longitudinal resonant mode ( $f_L^{(4)}$ ) and the eighth shear resonant mode ( $f_S^{(8)}$ ) for both bias field cases. Figure 5 presents the field dependences of their amplitudes. The amplitudes have been normalized by the maximum shear-wave amplitude in the normal bias field case. We have the following observations; (i) the shear-wave amplitude for the normal bias field shows the largest magnitude and (ii) it has a small peak in the lower field region; (iii)

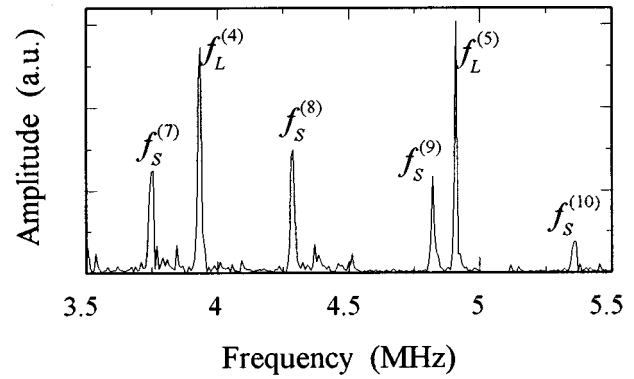
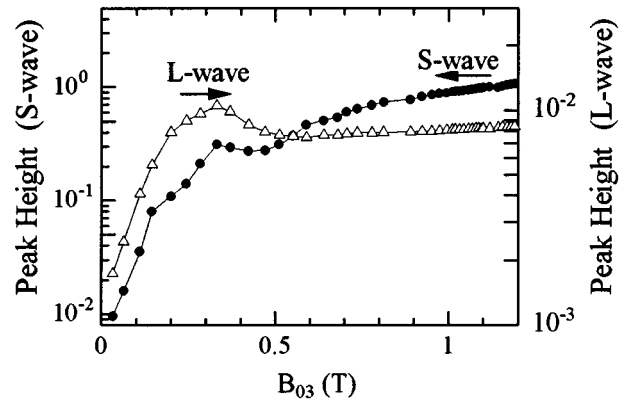
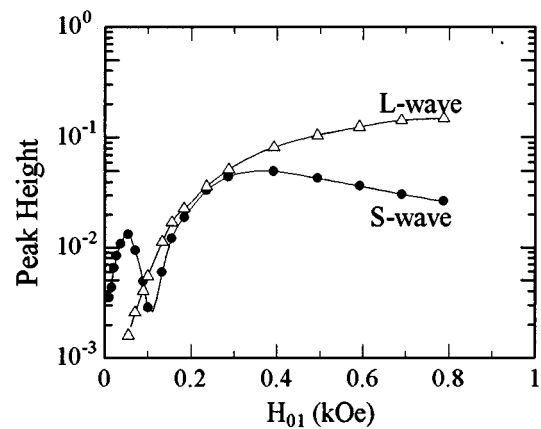


FIG. 4. EMAR spectra of the longitudinal and shear waves propagating in the thickness direction of the carbon steel plate (3 mm thick). The tangential field to the surface is 0.18 kOe.

the longitudinal-wave amplitude for the normal bias field increases with the field and after taking a maximum value, it becomes suitable up to 1.2 T; (iv) there are two peaks in the tangential-field dependence of the shear wave; and (v) the longitudinal-wave amplitude monotonously increases for the tangential field case. Since the Lorentz force and the magne-



(a) normal bias field



(b) tangential bias field

FIG. 5. Field dependences of the spectrum-peak height for the steel plate. Plotted are the response at the 4th resonant frequency for the longitudinal wave and the 8th one for the shear wave.

tization force mechanisms will cause the monotonous dependence as characterized by the magnetization curve, it is apparent that these mechanisms cannot explain the above observations.

#### IV. THEORETICAL ANALYSIS

##### A. Modeling

The basic equations governing the coupling of the electromagnetic field and the elastic deformation  $\mathbf{u}$  are given by<sup>5-8</sup>

$$\rho \frac{\partial^2 \mathbf{u}}{\partial t^2} = \nabla \cdot \mathbf{T} + \mathbf{f}, \quad (1)$$

$$\text{rot} \mathbf{E} = - \frac{\partial \mathbf{B}}{\partial t}, \quad (2)$$

$$\text{rot} \mathbf{H} = \frac{\partial \mathbf{D}}{\partial t} + \mathbf{J}, \quad (3)$$

$$\mathbf{E} = \sigma^{-1} \mathbf{J} + \frac{\partial \mathbf{u}}{\partial t} \times \mathbf{B}_0, \quad (4)$$

$$\mathbf{B} = \mu_0 \mu (\mathbf{H} - \mathbf{M}_0 \nabla \cdot \mathbf{u}) + e \cdot \epsilon'', \quad (5)$$

where  $\mathbf{E}$  is the electric field,  $\mathbf{B}$  the magnetic flux density,  $\mathbf{H}$  the magnetizing field,  $\mathbf{D}$  the dielectric displacement,  $\mathbf{J}$  the current density,  $\rho$  the mass density,  $\mathbf{T}$  the elastic stress tensor, and  $\mathbf{f}$  the body force per unit volume. They are all time-dependent quantities.  $\mathbf{B}_0$  and  $\mathbf{M}_0$  are the bias magnetic flux density and the bias magnetization.  $\sigma$  and  $\mu_0$  are the electrical conductivity and the free-space permeability.  $\mu$ ,  $e$ , and  $\epsilon''$  are tensors of the differential magnetic permeability, the inverse-magnetostriction constants, and the strain caused by the ultrasonic, respectively. The terms involving  $\mathbf{u}$  and  $\epsilon''$  in Eqs. (4) and (5) are only considered in the receiving process.

Some approximations are used for simplification. The rest of this section summarizes the formulation and the assumptions, including the magnetization curve, the anisotropic permeability, and the magnetostriction curve.

The electromagnetic and the elastodynamic fields are variables in the two-dimensional space of the  $x_1 - x_3$  plane. The half space of  $x_3 > 0$  is filled with a ferromagnetic metal, in which the  $x_1 - x_2$  plane defines the interface with vacuum. The bias field is homogeneous being normal or parallel to the surface. The magnetostriction causes no volume change (isovolume); this is true for an isotropic polycrystalline metal, because the randomly oriented easy axes average out the anisotropy of the magnetostriction of individual magnetic domains.<sup>14</sup> We also assume that the displacement current is neglected because of the relatively low frequency range and the magnetic states are reversibly changed through the rotation of the magnetization.

The formula presented by Potter and Schulian<sup>15</sup> is used to express the static response of the magnetization ( $M$ :T) to the field ( $H$ :kOe):

$$M = 2.2(0.27 - 0.73 \tanh(0.38 - 8.6 H)), \quad (6)$$

which is derived as the initial magnetization curve of the material with the saturation magnetization of 2.2 T and the

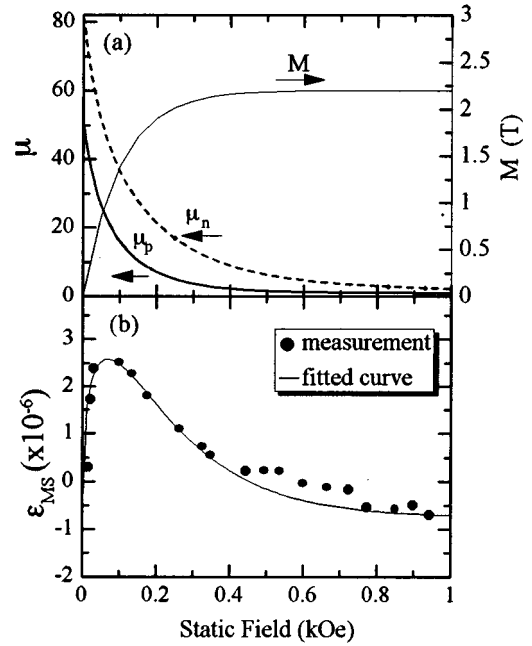


FIG. 6. (a) Simplification of the initial magnetization curve and calculated permeabilities, and (b) magnetostriction curve based on the measurements.

residual magnetization of 0.8 T [Fig. 6(a)]. This is an acceptable approximation for the practical initial magnetization curve of a low carbon steel.

With the magnetic anisotropy induced by the bias field, the nonzero components in the permeability tensor  $\mu$  in Eq. (5) are equal to  $\mu_p$  or  $\mu_n$ , which is the permeability parallel or normal to the bias field, respectively. Generally, the anisotropy originates from the rotation of the magnetization and the movement of the domain walls. But, because the material is magnetized by the dynamic field with a high frequency and a small amplitude in the EMAT phenomena, the domain walls will not oscillate responding to the field vibration. Only the rotation of the magnetization is then considered. The anisotropic permeability tensor is calculated following Chikazumi.<sup>14</sup> In a domain of a ferromagnetic metal with the cubic crystallographic symmetry, the magnetic energy is expressed by

$$U = K_1 \cos^2(\phi_0 - \phi) \sin^2(\phi_0 - \phi) - M_s H \cos \phi, \quad (7)$$

when the magnetization rotates in the plane involving an easy axis.  $K_1$  is the first magnetic anisotropy constant and  $M_s$  is the saturation magnetization.  $\phi$  and  $\phi_0$  are angles between the field and the magnetization and between the field and the easy axis. The stable direction is determined by minimizing the energy, that is,  $\partial U / \partial \phi = 0$ . The magnetization parallel and normal to the external field  $H$  is obtained by  $M_s \cos \phi$  and  $M_s \sin \phi$ . The values for  $\mu_p$  and  $\mu_n$  are given by differentiating  $M_p$  and  $M_n$  with respect to  $H$ , that is  $\mu_p = \partial(M_s \cos \phi) / \partial H$  and  $\mu_n = \partial(M_s \sin \phi) / \partial H$ . Because a polycrystalline metal is composed of the randomly oriented grains, the permeabilities are determined by averaging  $\mu_p$  and  $\mu_n$  for all possible angles of  $\phi_0$ . Figure 6(a) shows the permeabilities thus calculated.

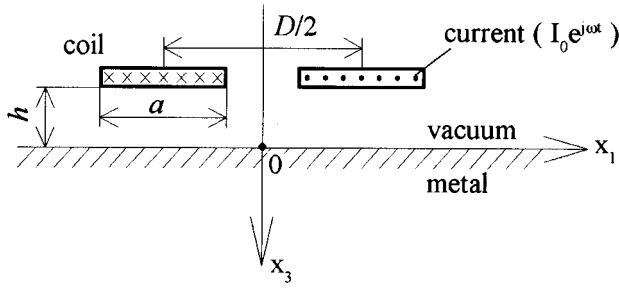


FIG. 7. Two-dimensional model to explain the electromagnetic phenomena caused by driving the spiral elongated coil.

Magnetostriction ( $\epsilon_{MS}$ ) is measured with the steel plate used in the field-dependence experiment and is approximated by

$$\epsilon_{MS} = 8H^{0.395} \cdot 1.79^{(-10H+1)} - 0.75, \quad (8)$$

where  $\epsilon_{MS}$  is in unit of microstrain and  $H$  in kOe. Figure 6(b) compares the measurement and the fitted function.

## B. Generation mechanism

The elastic wave field excited in the metal is governed by Eq. (1) with an electromagnetic body force  $\mathbf{f}$ , which can be expressed by the summation of the Lorentz force  $\mathbf{f}^{(L)}$ , the magnetization force  $\mathbf{f}^{(M)}$ , and the magnetostriction force  $\mathbf{f}^{(MS)}$ <sup>3,8</sup> as

$$\mathbf{f}^{(L)} = \mathbf{J}_e \times \mathbf{B}_0, \quad (9)$$

$$\mathbf{f}^{(M)} = (\nabla \mathbf{H}) \cdot \mathbf{M}_0, \quad (10)$$

$$\mathbf{f}^{(MS)} = \nabla \cdot (\mathbf{e} \cdot \mathbf{H}), \quad (11)$$

where  $\mathbf{J}_e$  is the eddy current density and  $\mathbf{e}$  is the tensor of the magnetostriction constants. The traction force  $T_{33}^{(M)}$  normal to the surface per unit area due to the bias magnetization also contributes to the wave generation:

$$T_{33}^{(M)} = \frac{1}{\mu_0} M_{03} M_n, \quad (12)$$

where  $M_n$  denotes the normal component at the surface of the magnetization of the metal. This term occurs as a result of the steep change of the electromagnetic field near the surface of a magnetized metal.<sup>16</sup> Because the forces in Eqs. (9)–(12) are caused by the electromagnetic fields in the metal, the calculation of the wave amplitude starts with deriving the fields in the metal induced by the driving current.

We consider the electromagnetic transduction with a harmonic excitation in a two-dimensional half-space occupied by an isotropic polycrystalline (Fig. 7). Coil elements are located near the surface with a liftoff  $h$ , and driven by the current of  $I_0 e^{j\omega t}$ ,  $\omega$  being angular frequency. The expression of  $e^{j\omega t}$  is omitted hereafter. Analogous procedure to the previous work<sup>3</sup> leads to the Fourier transform expression of the sheet current  $K(x_1, -h)$  per unit length along the  $x_1$  axis:

$$K(x_1, -h) = \frac{I_0}{a} \sum_{m=0}^{\infty} \left[ (-1)^m \frac{4}{(2m+1)} \times \sin\left(\frac{a}{2} k_m\right) \sin k_m x_1 \right], \quad (13)$$

where  $k_m = 2\pi(2m+1)/D$  is characteristic to the spiral-coil dimensions. Substituting Eq. (5) into Eq. (3), and eliminating the electric field with Eq. (4), we find that the magnetic field  $\mathbf{H}^V$  in vacuum satisfies Laplace's equation. It is easily solved with the boundary condition of  $H_1^V = K/2$  at  $x_3 = -h$ . In the metal region, a similar procedure reduces the simultaneous Eqs. (2)–(5) to a second-order differential equation for  $H_1$  by using  $\partial^2 H_1 / \partial x_1^2 = -k_m^2 H_1$ . The general solution of  $H_1$  contains a complex amplitude that is determined by the continuity of the tangential field at the boundary between the vacuum and metal regions ( $H_1^V = H_1$  at  $x_3 = 0$ ).  $H_3$  is also obtained from  $H_1$  by Eqs. (2) and (5). The solutions thus derived consist of a series of terms including  $e^{-2\pi(2m+1)h/D}$  and they decrease as  $m$  becomes larger. For focussing on the primary effect, the terms in the higher orders ( $m > 0$ ) are neglected in the following analysis. This is allowable for a large liftoff. The resultant expressions become

$$H_1 = -j \frac{2I_0}{a\pi} \sin\left(\frac{a}{D} \pi\right) e^{qx_3} e^{jk_0 x_1} e^{-k_0 h}, \quad (14)$$

$$H_3 = -\frac{\mu_{11}}{\mu_{33}} \frac{k_0}{q} \frac{2I_0}{a\pi} \sin\left(\frac{a}{D} \pi\right) e^{qx_3} e^{jk_0 x_1} e^{-k_0 h},$$

$$k_0 = 2\pi/D, \quad q = -(\alpha + j\alpha^{-1})/\delta,$$

$$\delta = \sqrt{2/(\sigma\omega\mu_0\mu_{11})}, \quad \alpha = \sqrt{(k_0\delta)^2(\mu_{11}/\mu_{33})/2+1}. \quad (15)$$

### 1. Lorentz force and magnetization force

The Lorentz force  $\mathbf{f}^{(L)}$  and the magnetization force  $\mathbf{f}^{(M)}$  are obtained by substituting Eqs. (14) and (15) into Eqs. (3), (9), and (10):

$$f_1^{(L)} + f_1^{(M)} = C_{11}^{(L)} \frac{\partial H_1}{\partial x_3} + C_{13}^{(M)} \frac{\partial H_3}{\partial x_3} - (B_{03} - M_{03}) \frac{\partial H_3}{\partial x_1}, \quad (16)$$

$$f_3^{(L)} + f_3^{(M)} = (C_{31}^{(L)} + C_{31}^{(M)}) \frac{\partial H_1}{\partial x_3} + C_{33}^{(M)} \frac{\partial H_3}{\partial x_3} + (B_{01} + M_{01}) \frac{\partial H_3}{\partial x_1},$$

$$C_{11}^{(L)} = B_{03}, \quad C_{31}^{(L)} = -B_{01},$$

$$C_{13}^{(M)} = -(\mu_{33}/\mu_{11})M_{01}, \quad C_{31}^{(M)} = M_{01}, \quad \text{and}$$

$$C_{33}^{(M)} = M_{03}, \quad (17)$$

where  $C_{ij}$  represents the coefficient of the body force  $f_i$  proportional to  $\partial H_j / \partial x_3$  or the gradient of the dynamic field  $H_j$  in the  $x_3$  direction. The terms involving  $\partial H_3 / \partial x_1$  are small enough compared with others; they will be neglected in the following discussions. Considering that  $H_1$  is much larger than  $H_3$  in magnitude and the well known relation of  $\mathbf{B}_0$

$= \mu_0 \mathbf{H} + \mathbf{M}_0$ , we find that  $f_3^{(L)}$  and  $f_3^{(M)}$  act in the opposite directions and  $f_3^{(M)}$  cancels the major part of  $f_3^{(L)}$ , that is,  $C_{31}^{(L)} + C_{31}^{(M)} = -\mu_0 H_{01}$ . The magnitude of  $\mu_0 H_{01}$  is much smaller than  $M_{01}$  in the field region used in the experiments, implying the small contribution of  $f_3^{(L)} + f_3^{(M)}$  to the elastic wave generation. This cancellation has been pointed out by Thompson<sup>5</sup> experimentally and by Il'in and Kharitonov<sup>6</sup> theoretically.

## 2. Magnetostrictive force

In case of the magnetic metals, the magnetization leads to the dimensional change in the magnetization direction, which is called magnetostriction. Magnetostriction changes with the dynamic field, resulting in the ultrasonic source.

The magnetostriction constant  $e_{k,ij}$  in Eq. (11) represents the dynamic response of the magnetostrictive stress  $\sigma_{ij}$  to the field  $H_k$ . Using the magnetostriction  $\epsilon_{mn}$  which depends on the total field,  $e_{k,ij}$  is expressed as follows:<sup>5,17</sup>

$$e_{k,ij} \equiv \left( \frac{\partial \sigma_{ij}}{\partial H_k} \right) = \left( \frac{\partial \sigma_{ij}}{\partial \epsilon_{mn}} \right)_{|H=0} \left( \frac{\partial \epsilon_{mn}}{\partial H_k} \right)_{|\sigma=0}, \quad (18)$$

where  $(\partial \sigma_{ij} / \partial \epsilon_{mn})_{H=0}$  can be replaced by the elastic stiffness. In Eq. (18), the summation convention is implied. Equation (18) indicates that the strain due to the magnetic field (i.e., magnetostriction) is regarded to be equivalent to the strain caused by the stresses without the field.

It is difficult to determine  $e_{k,ij}$  by experiments. Il'in and Kharitonov<sup>6</sup> and Wilbrand<sup>7</sup> used a rough approximation for it; Thompson<sup>5</sup> derived it from the slope of magnetostriction response to the bias field. The present analysis, however, takes account of the magnetostriction change responding to the total field, which is very important for the wave generation as will be shown later.

When the dynamic field is superimposed on the bias field, the total field is inclined from the original direction. Because the magnetostriction tends to occur in both the parallel and normal directions to the total field, we should consider the principal coordinate system to calculate  $\sigma_{ij}$ . Considering a new system  $(x'_1, x'_2, x'_3)$  where the total magnetic field lies along the  $x'_1$  direction and  $x'_2 = x_2$ , only three principal stresses ( $\sigma'_{11}$ ,  $\sigma'_{22}$ , and  $\sigma'_{33}$ ) exist. Because of the iso-volume magnetostriction, the magnitude of the magnetostriction along the applied field is twice larger than those in the perpendicular directions, being in the opposite sign. Supposing  $\partial \epsilon'_{22} / \partial H'_1 = \partial \epsilon'_{33} / \partial H'_1 = -(\partial \epsilon'_{11} / \partial H'_1) / 2$  and using Hooke's law, Eq. (18) is reduced to

$$\left. \begin{aligned} \partial \sigma'_{11} / \partial H'_1 &= 6 \kappa G \\ \partial \sigma'_{22} / \partial H'_1 &= -3 \kappa G \\ \partial \sigma'_{33} / \partial H'_1 &= -3 \kappa G \end{aligned} \right\}, \quad (19)$$

where  $G$  is the shear modulus and  $\kappa = \partial \epsilon'_{11} / \partial H'_1$  is a function of the total field and given from the slope of the magnetostriction curve in Fig. 6(b). Introducing the direction cosine  $Q_{ij}$  between the  $x'_i$  and  $x_j$  axes, we have  $\sigma_{ij} = \sigma'_{mn} Q_{mi} Q_{nj}$ . In the present two-dimensional model,  $Q_{ij}$  are calculated using an angle  $\theta$  between the total field and the bias field, and we have

$$\begin{aligned} \sigma_{11} &= \sigma'_{11} \sin^2 \theta + \sigma'_{33} \cos^2 \theta, \\ \sigma_{33} &= \sigma'_{11} \cos^2 \theta + \sigma'_{33} \sin^2 \theta, \\ \sigma_{13} &= (\sigma'_{11} - \sigma'_{33}) \sin \theta \cos \theta, \end{aligned} \quad (20)$$

for a normal bias field, and

$$\begin{aligned} \sigma_{11} &= \sigma'_{11} \cos^2 \theta + \sigma'_{33} \sin^2 \theta, \\ \sigma_{33} &= \sigma'_{11} \sin^2 \theta + \sigma'_{33} \cos^2 \theta, \\ \sigma_{13} &= (\sigma'_{11} - \sigma'_{33}) \sin \theta \cos \theta, \end{aligned} \quad (21)$$

for a tangential bias field. The magnetostriction constants  $e_{k,ij}$  are obtained from Eqs. (18)–(21) for each of the normal and the tangential fields:

(i) normal bias field

$$\left. \begin{aligned} e_{1,11} &= 3 \kappa G \sin \theta (2 \sin^2 \theta - \cos^2 \theta) + \frac{6G\epsilon'_{11}}{H_{03}} \cos^3 \theta \sin \theta, \\ e_{1,13} &= 9 \kappa G \sin^2 \theta \cos \theta + \frac{3G\epsilon'_{11}}{H_{03}} \cos 2\theta \cos^2 \theta, \\ e_{1,33} &= 3 \kappa G \sin \theta (2 \cos^2 \theta - \sin^2 \theta) - \frac{6G\epsilon'_{11}}{H_{03}} \cos^3 \theta \sin \theta, \\ e_{3,11} &= -3 \kappa G, \quad e_{3,13} = 0, \quad e_{3,33} = 6 \kappa G \\ \theta &= \tan^{-1}(H_1/H_{03}) \end{aligned} \right\}, \quad (22)$$

(ii) tangential bias field

$$\left. \begin{aligned} e_{1,11} &= 6 \kappa G, \quad e_{1,13} = 0, \quad e_{1,33} = -3 \kappa G \\ e_{3,11} &= 3 \kappa G \sin \theta (2 \cos^2 \theta - \sin^2 \theta) - \frac{6G\epsilon'_{11}}{H_{01}} \cos^3 \theta \sin \theta, \\ e_{3,13} &= 9 \kappa G \sin^2 \theta \cos \theta + \frac{3G\epsilon'_{11}}{H_{01}} \cos 2\theta \cos^2 \theta, \\ e_{3,33} &= 3 \kappa G \sin \theta (2 \sin^2 \theta - \cos^2 \theta) + \frac{6G\epsilon'_{11}}{H_{01}} \cos^3 \theta \sin \theta \\ \theta &= \tan^{-1}(H_3/H_{01}). \end{aligned} \right\}, \quad (23)$$

The body force  $\mathbf{f}^{(MS)}$  due to the magnetostriction effect is determined by

$$f_i^{(MS)} = \partial \sigma_{ij} / \partial x_j = e_{k,ij} (\partial H_k / \partial x_j), \quad (24)$$

and we can define coefficients  $C_{ij}^{(MS)}$  like in Eqs. (16) and (17) as follows

$$\left. \begin{aligned} C_{11}^{(MS)} &= e_{1,13}, \quad C_{13}^{(MS)} = -\frac{\mu_{33}}{\mu_{11}} e_{1,11}, \\ C_{31}^{(MS)} &= e_{1,33}, \quad C_{33}^{(MS)} = e_{3,33} - \frac{\mu_{33}}{\mu_{11}} e_{1,13} \end{aligned} \right\}, \quad \text{normal bias field,} \quad (25)$$

$$\left. \begin{aligned} C_{11}^{(MS)} &= 0, \quad C_{13}^{(MS)} = -\frac{\mu_{33}}{\mu_{11}} e_{1,11} + e_{3,13}, \\ C_{31}^{(MS)} &= e_{1,33}, \quad C_{33}^{(MS)} = e_{3,33} \end{aligned} \right\}, \quad \text{tangential bias field.} \quad (26)$$

It should be noted that if the inclination of the total field was ignored ( $\sigma_{13} = 0$ ), the expressions for  $e_{k,ij}$  would be

quite different from the above results; especially,  $e_{1,13}$  would vanish in the case of the normal bias field. However, in the present model,  $e_{1,13}$  takes a large value even in the high field limit of  $\theta = 0$  in Eq. (22) and contributes to  $f_1^{(MS)}$ .

### 3. Wave amplitude

Body forces obtained in Eqs. (16), (17), and (24) are coupled to the bulk waves in Eq. (1). Taking the longitudinal wave for example, Eq. (1) is reduced to the second-order differential equation by noting  $\partial^2 u_3 / \partial x_1^2 = -k_0^2 u_3$ :

$$\frac{\partial^2 u_3}{\partial x_3^2} + (k_3^2 - k_0^2)u_3 = -\frac{f_3}{\lambda + 2G}, \quad (27)$$

$$k_3 = \omega/c_L, \quad c_L = \sqrt{(\lambda + 2G)/\rho},$$

where  $\lambda$  is one of Lamé's constants. Particular solution is first obtained and then the general solution is expressed by the summation of the particular solution and the homogeneous solution. The general solution includes an unknown constant, which is determined by the stress-free condition at  $x_3 = 0$  together with Eq. (12). The resultant expression of the general solution consists of two terms; one is proportional to  $e^{-\alpha x_3/\delta}$  and rapidly decays in the thickness direction. The other term carries energy into the metal and represents the generated ultrasonic wave. The expression of the term for the longitudinal wave is

$$u_3 = \frac{2I_0 \sin(\alpha\pi/D)}{\alpha\pi K(\lambda + 2G)} \left[ \left( \frac{\mu_{11}}{\mu_{33}} \Delta_0(\Delta_3^2 - \Delta_0^2 - 2)C_{33} - 4C_{31} \right) + j \left( \frac{\mu_{11}}{\mu_{33}} \Delta_0(\Delta_3^2 - \Delta_0^2 + 2)C_{33} + 2(\Delta_3^2 - \Delta_0^2)C_{31} \right) \right] e^{j(-Kx_3 + k_0 x_1)}, \quad (28)$$

where  $\Delta_0 = k_0 \delta$ ,  $\Delta_3 = k_3 \delta$ , and  $K^2 = k_3^2 - k_0^2$ . A similar procedure leads to the solution for the shear wave.

The ultrasonic amplitude thus derived will be in the form

$$u_i = u_i^{(L)} + u_i^{(M)} + u_i^{(MS)}, \quad i = 1 \text{ or } 3. \quad (29)$$

and the contribution of each mechanism for the elastic wave generation can be discussed separately. Figure 8 shows the field dependence of the bulk-wave amplitudes due to the magnetostrictive effect normalized by the Lorentz force contribution for the longitudinal wave ( $|u_i^{(MS)}|/|u_3^{(L)}|$ ) for each bias field. Used parameters are as follows;  $f = 4$  MHz,  $D = 20$  mm,  $a = 4.5$  mm,  $h = 0.5$  mm,  $I_0 = 50$  A,  $G = 80$  GPa,  $\lambda = 120$  GPa,  $\sigma = 3.3 \times 10^6$  S/m, and  $\mu_0 = 1.26 \times 10^{-6}$  H/m, which are compatible with the experimental condition. The contributions of the magnetization mechanism and that of the tangential Lorentz force are not included in Fig. 8 because of the similarity to the vertical Lorentz force case ( $|u_1^{(L)}| \sim [(\lambda + 2G)/G]|u_3^{(L)}|$ ,  $|u_3^{(M)}| \sim |u_3^{(L)}|$ ,  $|u_1^{(M)}| \ll |u_3^{(L)}|$ ).

Figure 8 indicates a much larger contribution of the magnetostriction effect than the others, especially in the lower field region. As the external field increases, the contributions of the Lorentz force and the magnetization force become considerable. The bias field exerted by a permanent magnet in a low carbon steel is usually less than 0.5 kOe,<sup>18</sup>

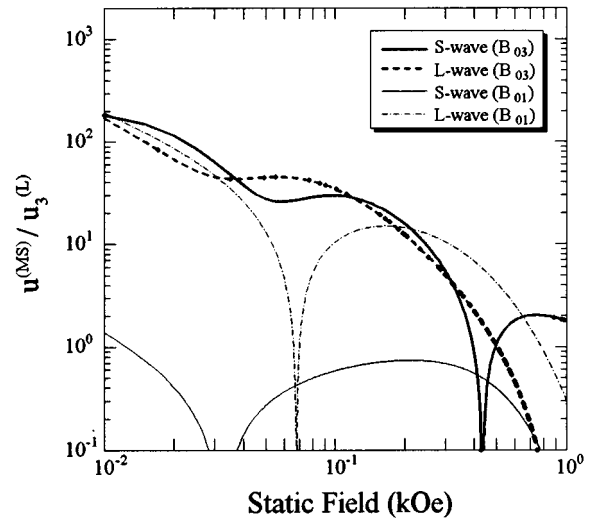


FIG. 8. Calculation of the field dependence of the generated bulk-wave amplitudes.

suggesting that the magnetostriction mechanism governs the bulk-wave generation as a whole, regardless of the field direction. We also find the smaller generation efficiency in the tangential bias field than in the normal bias field. Especially, the efficiency of the shear-wave generation in the tangential bias field is the smallest. The shear wave amplitude  $|u_1^{(MS)}|$  in the tangential field case is nearly proportional to  $\Delta_0 (= k_0 \delta)$ . The neglect of the higher-order terms in the Fourier transform expression of the dynamic field has smoothed out the steep change of the field around the center region of the coil elements ( $x_1 \sim 0$ ). This decrease  $k_0$  and therefore underestimates the shear wave amplitude. But the field dependence is not so affected by this neglect because it mainly depends on the field dependence of the permeability, the magnetization, and the magnetostriction response.

### C. Receiving mechanism

The excited ultrasonic wave travels in the thickness direction, is reflected at the bottom surface, and then returns to the incident surface. Because of the inverse magnetostriction effect, the elastic deformation due to the ultrasonic wave disturbs the electromagnetic field, giving rise to the dynamic fields. The coupling occurs at the boundary between the metal and vacuum regions and the excited field are detected by the coil element placed in the vacuum region. Il'in and Kharitonov<sup>6</sup> calculated the electric field in the vacuum region induced by the Rayleigh waves. Their procedure is applied here for calculating the electric field induced in the vacuum region by the bulk waves, although the derivation of the inverse-magnetostriction constants has been modified from their analysis.

The inverse-magnetostriction constants  $e_{k,ij}$  in Eq. (5) represent the generation ratio of the magnetic flux density  $B_k$  induced by the elastic strain  $\epsilon_{ij}$ :<sup>17</sup>

$$e_{k,ij} = \left( \frac{\partial B_k}{\partial \epsilon_{ij}} \right) = \mu_{kk} \left( \frac{\partial H_k}{\partial \epsilon_{ij}} \right). \quad (30)$$

Summation is not implied by the repeated indices. Uniform bias field causes the orthogonal anisotropy in the magnetic properties of a ferromagnetic material that is originally isotropic. One of the principal axes coincides with the field direction. Therefore, only three inverse-magnetostriction constants have to be taken into account. They are denoted by  $e_{33}$ ,  $e_{31}$ , and  $e_{15}$ .  $e_{33}$  is the constant for the parallel magnetic induction to the bias field due to the principal strain along the bias field;  $e_{31}$  the constant for the parallel magnetic induction due to the principal strain normal to the field, and  $e_{15}$  the constant for the normal magnetic induction to the bias field due to the shear strain  $\epsilon_{13}$ .  $e_{31}$  is approximated by  $-\nu e_{33}$  by noting  $\partial H_3/\partial \epsilon_{11} = (\partial H_3/\partial \epsilon_{33})(\partial \epsilon_{33}/\partial \epsilon_{11})$ , where  $\nu$  is Poisson's ratio.

Considering the bias field direction and the wave mode, the calculation of receiving efficiency is carried out for four cases:

- (i)  $\mathbf{u} = (u_1 e^{j(k_3 x_3 + k_0 x_1)}, 0, 0)$  and  $\mathbf{B} = (0, 0, B_{03})$
- (ii)  $\mathbf{u} = (u_1 e^{j(k_3 x_3 + k_0 x_1)}, 0, 0)$  and  $\mathbf{B} = (B_{01}, 0, 0)$
- (iii)  $\mathbf{u} = (0, 0, u_3 e^{j(k_3 x_3 + k_0 x_1)})$  and  $\mathbf{B} = (0, 0, B_{03})$
- (iv)  $\mathbf{u} = (0, 0, u_3 e^{j(k_3 x_3 + k_0 x_1)})$  and  $\mathbf{B} = (B_{01}, 0, 0)$ .

For example, case (i) is explained in the following. This is the case that the shear wave polarized in the  $x_1$  direction is impinged on the surface region where the normal bias field is present. In the metal region, substituting Eq. (5) into Eq. (2) and eliminating  $H_1$  and  $H_3$  using Eqs. (3) and (4), we obtain a differential equation for  $E_2$ :

$$\frac{\partial^2 E_2}{\partial x_3^2} - q^2 E_2 = B_{03} \omega u_1 - j \left\{ \left( k_3^2 e_{15} - \frac{\mu_{33}}{\mu_{11}} k_1^2 \right) + k_1^2 \mu_{11} M_{03} \right\} \omega u_1, \quad (31)$$

$$q^2 = \frac{\mu_{33}}{\mu_{11}} k_1^2 + j \frac{2}{\delta^2}.$$

The particular solution in the form of  $E_2 = A e^{j(k_3 x_3 + k_0 x_1)}$  is

considered, and the complex amplitude  $A$  is determined by substituting it into Eq. (31). The general solution takes the form of  $E_2 = (C e^{q x_3} + A e^{j k_3 x_3}) e^{j k_0 x_1}$  with unknown  $C$ . On the other hand, Eq. (31) takes the following form in the vacuum region

$$\frac{\partial^2 E_2^V}{\partial x_3^2} - k_0^2 E_2^V = 0, \quad (32)$$

and the solution is  $E_2^V = D e^{k_0 x_3} e^{j k_0 x_1}$ . The unknown complex amplitudes  $C$  and  $D$  are determined by the boundary condition at the surface, which moves responding to the elastic wave:

$$\mathbf{n}_0 \times (\mathbf{E}^V - \mathbf{E}) = V_3 (\mathbf{B}_0^V - \mathbf{B}_0), \quad (33)$$

$$\mathbf{n}_0 \times (\mathbf{H}^V - \mathbf{H}) + \mathbf{n}' \times (\mathbf{H}_0^V - \mathbf{H}_0) = 0, \quad (34)$$

where  $\mathbf{n}_0$  is an outward unit vector normal to the surface and  $\mathbf{n}'$  is the one when the surface is displaced by the ultrasonic wave.  $V_3$  is the normal component of the particle velocity at the boundary. From these relations, we have the electric field  $E_2^V$  and it is expressed by the contribution of each mechanism:

$$E_2^V = E^{(L)} B_{03} + E^{(M)} M_{03} + E^{(MS1)} e_{15} + E^{(MS2)} e_{33}, \quad (35)$$

where

$$\left. \begin{aligned} E^{(L)} &= -\frac{\tau}{2\xi} [(-\eta\chi + 2\zeta) + j(\zeta\chi + 2\eta)] \omega u_1 \\ E^{(MS1)} &= \frac{\Delta_3}{4\xi} [(2\eta\kappa\Delta_3 + \zeta\kappa\chi\Delta_3 + 4\beta) + j(-2\zeta\kappa\Delta_3 + \eta\kappa\chi\Delta_3 - 4/\alpha)] \omega u_1 \\ E^{(MS2)} &= \frac{\nu\tau\Delta_1^2}{4\xi} \frac{\mu_{11}}{\mu_{33}} [(2\eta + \zeta\chi) + j(-2\zeta + \eta\chi)] \omega u_1 \\ E^{(M)} &= \frac{\tau\Delta_1^2\mu_{11}}{4\xi} [(2\eta + \zeta\chi) + j(-2\zeta + \eta\chi)] \omega u_1 \end{aligned} \right\}, \quad (36)$$

and

$$\left. \begin{aligned} \chi &= \Delta_3^2 + \frac{\mu_{11}}{\mu_{33}} \Delta_1^2, & \tau &= (1 + \chi^2/4)^{-1}, & \xi &= \beta^2 + \alpha^{-2}, \\ \eta &= \alpha\beta + \gamma\alpha^{-1}, & \zeta &= 1 - \beta\gamma, & \beta &= \alpha + \mu_{11}\Delta_1, & \gamma &= \alpha^{-1} + \Delta_3 \end{aligned} \right\}. \quad (37)$$

Similar analysis allows us to calculate  $E_2^V$  in other cases.

The field dependence of the coefficients in Eq. (36) are calculated with the parameters used in Fig. 8. Their results are summarized as follows. For all cases,  $|E^{(L)}|$  or  $|E^{(M)}|$  is about ten times larger than  $|E^{(MS1)}|$  or  $|E^{(MS2)}|$  in the lower field region, but all of them get closer as the field increases. However, noting  $B_0 \sim M_0 < M_s$  and  $e_{33}, e_{15} \gg M_s$  for steels,<sup>7,17</sup> it is considered that the contributions of the magnetostriction mechanism to the reception will be larger than the Lorentz force and the magnetization force mechanisms. We also find that  $|E^{(MS1)}|$  for the shear wave in the normal field [case (i)] is the largest among  $|E^{(MS1)}|$  and  $|E^{(MS2)}|$ .

The detailed calculation of the field dependence of the receiving efficiency requires the dynamic response of  $e$  at a bias field. Unlike the magnetostriction constants, the response of the inverse-magnetostriction constants are not easily estimated from the experimental data, because it is difficult to measure the magnetic induction due to a deformation in a static field. Furthermore, the dynamic response of the induction caused by the small deformation due to the elastic waves will not be measurable. In this situation, the magnetostriction data in Fig. 6(b), which is useful for calculating the generation efficiency, is still used to estimate  $e_{15}$  and  $e_{33}$  in following discussion.

Consider that the external field  $H_{03}$  is applied to the  $x_3$  direction and the strain  $\epsilon_{33}^u$  is introduced by the longitudinal wave. The total strain along the  $x_3$  direction becomes  $\epsilon_{MS}(H_{03}) + \epsilon_{33}^u$ , where  $\epsilon_{MS}(H)$  is the magnetostriction along the total field. This is considered to be equivalent to the strain that arises when the perturbation field  $H_3$  occurs in the  $x_3$  direction and the magnetostriction is changed to  $\epsilon_{MS}(H_{03} + H_3)$  without the elastic wave. If  $H_3$  is small enough compared with  $H_{03}$ , we have  $\epsilon_{33}^u = \partial \epsilon_{33} / \partial H_3$ , and then

$$e_{33} = \mu_0 \mu_{33} \left( \frac{\partial \epsilon_{33}}{\partial H_3} \right)^{-1} = \mu_0 \mu_{33} \kappa^{-1}. \quad (38)$$

Next, consider the shear strain  $\epsilon_{13}^u$  caused by the elastic wave. This is again equivalent to the strain that arises when the perturbation field  $H_1$  occurs normal to the bias field without the elastic deformation and the principal coordinate system rotates from the original. The strain due to the magnetostriction in the principal coordinate system will be  $\epsilon'_{33} = \epsilon_{MS}(H')$  and  $\epsilon'_{11} = -\epsilon'_{33}/2$ , where  $H' = \sqrt{H_{03}^2 + H_1^2}$ . In the original coordinate system, the shear strain is expressed by  $\epsilon_{13} = (\epsilon'_{11} - \epsilon'_{33}) \cos \theta \sin \theta$ , where  $\theta = \tan^{-1}(H_1/H_{03})$ . Assuming  $\epsilon_{13}^u = \epsilon_{13}$ , we derive

$$\epsilon_{13}^u = -\frac{3}{2} \epsilon_{MS}(H') \sin \theta \cos \theta. \quad (39)$$

By differentiating Eq. (39) with respect to  $\epsilon_{13}^u$  and assuming  $H_1$  to be small enough, we have

$$e_{15} = -\mu_0 \mu_{11} \frac{2}{3} \frac{H_{03}}{\epsilon_{MS}(H_{03})}. \quad (40)$$

Equations (38) and (40) allow us to calculate the field dependence of the receiving efficiency on the basis of Eq. (35).

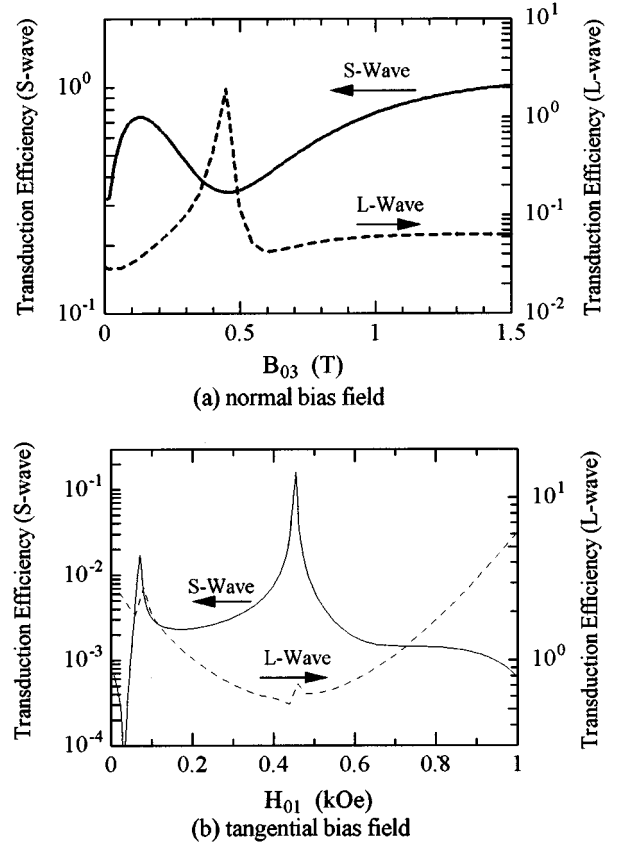


FIG. 9. Calculation of the field dependence of the bulk-waves generated and then detected by the EMAT.

#### D. Efficiency of the bulk-wave EMAT

The product of the generation efficiency ( $u/I_0$ ) from Eq. (29) and the receiving efficiency ( $E_2/u$ ) from Eq. (35) provides the field dependence of the total transduction efficiency with the EMAT. Figure 9 shows the transduction efficiencies of the four cases, which are normalized by the efficiency of the shear wave at the normal bias field of 1.5 T. These results can be compared with the measurements in Fig. 5. Although there are some discrepancies, the general features (i)–(iv) observed in Fig. 5 are well explained by the present model. The efficiency of the longitudinal wave for the tangential bias field [Fig. 9(b)] is not favorably compared with the measurement in Fig. 5 in the lower field region. This will be attributed to the rough estimation of the inverse-magnetostriction constants.

Figures 5 and 9 provide an explanation for the unsolved behavior with the bulk-wave EMAT, that is, much smaller transduction efficiency of the longitudinal wave, and its dependence on the sample thickness (Fig. 2). The efficiencies for the longitudinal wave for both bias fields are quite small compared to that of the shear wave for the normal field case, especially in the lower field region, indicating that the longitudinal wave is hardly detected. The efficiency, however, increases with the bias field. For a thick plate, the field is not strong enough because of the larger volume of the material to be magnetized and the shear wave are considerably larger; while for a thinner plate, the magnetic field is forced to con-

concentrate within the thin thickness, resulting in the higher field, and then the longitudinal wave becomes larger.

## V. CONCLUSION

The coupling mechanism between the bulk waves and the electromagnetic field has been discussed, experimentally and theoretically. The EMAR technique made it possible to measure the field dependence of the bulk-wave amplitudes in a thin plate by means of the resonant peaks, which would not be realized with the conventional pulse-echo technique because of the overlapping of echoes. The experiments showed different features of coupling, depending on the direction of the bias fields and the wave modes.

A theoretical model was presented to explain the complex field dependences in the carbon steel, in which the derivation of the magnetostriction constants and the inverse-magnetostriction constants has been improved from the previous work. The inclination of the total field due to the dynamic one is taken account in the present model and is found to be essential. Using several assumptions, the model explains the field dependencies of the coupling efficiency observed by the experiments.

As a consequence, the magnetostriction effect dominates the coupling phenomena both for the normal and tangential bias fields to the surface in ferromagnetic metals. The efficiency of the shear wave generation and detection for the normal bias is considerably larger than other cases, and that of the longitudinal wave is fairly small for both fields. This

explained the unsolved behavior of the bulk-wave EMAT. The knowledge given here will help us to improve the transduction efficiency of EMATs. For example, coating the surface with a thin film of substance having a large magnetostriction constants may lead to the dramatical improvement of the EMAT efficiency.

- <sup>1</sup>M. R. Gaertner, W. D. Wallace, and B. W. Maxfield, *Phys. Rev.* **184**, 702 (1969).
- <sup>2</sup>R. B. Thompson, *J. Appl. Phys.* **48**, 4942 (1977).
- <sup>3</sup>R. B. Thompson, *Physical Acoustics*, edited by R. N. Thurston and A. D. Pierce (Academic Press, New York, 1990), Vol. **19**, p. 157.
- <sup>4</sup>B. W. Maxfield and C. M. Fortunko, *Mater. Eval.* **41**, 1399 (1983).
- <sup>5</sup>R. B. Thompson, *IEEE Trans. Sonics Ultrason.* **SU-25**, 7 (1978).
- <sup>6</sup>I. V. Il'in and A. V. Kharitonov, *Sov. J. Nondestruct. Test.* **16**, 549 (1980).
- <sup>7</sup>A. Wilbrand, *New Procedures in Nondestructive Testing*, edited by P. Höller (Springer, Berlin, 1983), p. 71.
- <sup>8</sup>A. Wilbrand, *Review of Progress in QNDE*, edited by D. O. Thompson and D. E. Chimenti (Plenum, New York, 1987), Vol. 7, p. 671.
- <sup>9</sup>K. Kawashima, *J. Acoust. Soc. Am.* **87**, 681 (1990).
- <sup>10</sup>M. Hirao, H. Ogi, and H. Fukuoka, *Rev. Sci. Instrum.* **64**, 3198 (1993).
- <sup>11</sup>W. L. Johnson, B. A. Auld, and G. A. Alers, *J. Acoust. Soc. Am.* **95**, 1413 (1994).
- <sup>12</sup>H. Ogi, M. Hirao, and T. Honda, *J. Acoust. Soc. Am.* **98**, 458 (1995).
- <sup>13</sup>H. Ogi, M. Hirao, and K. Minoura, *J. Appl. Phys.* **81**, 3677 (1997).
- <sup>14</sup>S. Chikazumi, *Physics of Magnetism* (Wiley, New York, 1964).
- <sup>15</sup>R. I. Potter and R. J. Schmulian, *IEEE Trans. Magn.* **MAG-7**, 4 (1971).
- <sup>16</sup>S. Iida, *New Electromagnetic Dynamics*, Maruzen, 1975, in Japanese.
- <sup>17</sup>D. A. Berlincourt, D. R. Curran, and H. Jaffe, *Physical Acoustics*, edited by W. P. Mason (Academic, New York, 1964), Vol. 1A, p. 169.
- <sup>18</sup>H. Ogi, K. Minoura, and M. Hirao, *Trans. Jpn. Soc. Mech. Eng., Ser. A* **62**, 1955 (1996), in Japanese.